5th International Conference on Control Engineering&Information Technology (CEIT-2017)
Proceeding of Engineering and Technology –PET
Vol.34 pp.17-22

Attitude Control Design using Adaptive Generalized Dynamic Inversion for Multi-rotor Aerial Vehicle

Uzair Ansari
Aeronautical Engineering Department
King Abdulaziz University
Jeddah 21589, Saudi Arabia
Email: uzansari@hotmail.com

Abdulrahman H. Bajodah
Aeronautical Engineering Department
King Abdulaziz University
Jeddah 21589, Saudi Arabia
Email: abajodah@kau.edu.sa

***Abstract*—This paper presents the attitude control system design of multi-rotor aerial vehicle based on Adaptive Generalized Dynamic Inversion (AGDI). The two-loop structured control system is proposed, in which the outer loop utilizes Proportional Derivative control to provide the reference pitch and roll attitude commands to the inner loop, while controlling the desired altitude. For the inner loop attitude dynamics, the conventional Generalized Dynamic Inversion (GDI) control is constructed by prescribing the linear time varying constraint differential equation, based on the attitude deviation function and is inverted by utilizing Moore-Penrose Generalized Inverse to realize the control law. The null control is designed in the auxiliary part of GDI, to provide asymptotic stability of body rate dynamics. The singularity issue of GDI is addressed tactfully by incorporating a dynamic scale factor. Sliding Mode based robust term with adaptive modulation gain is integrated with GDI to make it AGDI, that guarantees semi-global practically stable attitude tracking. Numerical simulations are conducted on Quadrotor simulator to demonstrate the controller's performance.**

NOMENCLATURE

ω	Angular speed, rad/sec
b	Lift coefficient
τ	Torque, N-m
d	Moment arm, m
k	Drag coefficient
$\phi\ \theta\ \psi$	Euler roll, pitch, yaw attitudes, deg
m	Mass, kg
g	Acceleration due to gravity, m/sec^2
p, q, r	Body angular velocities, rad/sec

Subscript

d	Desired values

I. INTRODUCTION

Quadrotors belongs to a certain class of Unmanned Aerial Vehicles (UAVs) that is evolving as a popular research platform in the control community because of the simplicity of its design and low maintenance and operation cost. It delivers the UAVs with skills such as hovering and vertical take-off and landing. They have sufficient payload capability and flight time to support a various of indoor and outdoor applications, see [1].

The multi-rotor vehicles set new challenges for the engineers to design its control system [2]. In linear control algorithms, Proportional Integral Derivative (PID) and Linear Quadratic Regulator (LQR) [3], are very popular, however their performance might be degrade due to nonlinear behaviour of multi-rotor vehicles over wide range of operation. To cope with, many nonlinear control techniques are developed such as Back Stepping Control [4], Sliding Mode Control (SMC) [5], Fuzzy Logic Control [6], Model Predictive Control [7], Nonlinear Dynamic Inversion (NDI) [8], [9], etc.

In contrast to NDI, a new methodology that is based on inversion principle is Generalized Dynamic Inversion (GDI) control. This approach based on inverting a prescribed set of constraint dynamics that includes the control objectives, and are inverted using Moore-Penrose Generalized Inverse (MPGI) based Greville method. This will mitigate the presumptions taken in NDI for acquiring the inverse of the whole system. This control technique has been applied to several aerospace engineering and robotics applications see, [10], [11], [12], [13], [14], [15], [16], [17], [18], [19].

In this paper, a two-loop structured control system is proposed for autonomous operation of Quadrotor. In outer (position) loop, Proportional Derivative (PD) control is employed, which generates the desired pitch and roll attitude commands for the inner loop, to minimize longitudinal and lateral positional errors along with tracking the required altitude. In the inner loop, GDI is employed in which dynamic constraints are defined based on the attitude deviation function that encapsulates the control objectives, and are inverted by using MPGI based Greville formula. The singularity problem due to non-square inversion is addressed by augmenting a dynamic scale factor in MPGI. The body rate dynamics are stabilized by using Lyapunov based null control vector. Because dynamic inversion scaling deteriorates inner loop performance, a robust term based on SMC with adaptive modulation gain, is integrated with GDI to make it Adaptive Generalized Dynamic Inversion (AGDI). The proposed control guarantees uniformly ultimately bounded attitude trajectory tracking errors and semi-global practically stable attitude tracking. For performance evaluation, numerical simulations are conducted on 6 Degrees of Freedom (DOFs) simulator of X4-flyer Quadrotor in both nominal and perturbed flight conditions.

The remaining part of the paper is organized as follows. The

ISSN 2356-5608

modeling of the Quadrotor is presented in section II. The two-loop control architecture is explained in section III. The design of PD control for the outer position loop is discussed in section IV. The basic formulation of GDI attitude control system is shown in section V. The detailed design process of AGDI control is presented in section VI, which guarantees semi-global practically stable attitude tracking. Finally, simulation results and conclusion are presented in section VII, and VIII respectively.

II. Quadrotor Mathematical Modeling

For mathematical modeling two reference frames are used. The body fixed frame is represented by $B(x_b, y_b, z_b)$ and inertial Earth-fixed reference frame is denoted by $E(x_e, y_e, z_e)$ as shown in Fig. 1. The thrust force produced by the individual

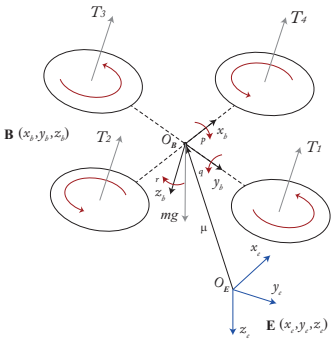

Fig. 1: Quadrotor configuration

rotor in the upward direction is written as

$$T_i = b\omega_i^2, \quad i = 1, 2, 3, 4 \tag{1}$$

The total thrust is given by

$$T = \sum_{i=1}^{4} T_i \tag{2}$$

The torques generated along x_b axis, the y_b axis, and the z_b axis are written as

$$\tau_x = db(\omega_4^2 - \omega_2^2) \tag{3}$$
$$\tau_y = db(\omega_3^2 - \omega_1^2) \tag{4}$$
$$\tau_z = k(\omega_1^2 - \omega_2^2 + \omega_3^2 - \omega_4^2) \tag{5}$$

The relation between input and output vector of Quadrotor is given as

$$\mathbf{u} = \mathbf{W}\begin{bmatrix}\omega_1^2 & \omega_2^2 & \omega_3^2 & \omega_4^2\end{bmatrix}^T \tag{6}$$

where $\mathbf{u} = \begin{bmatrix}T & \tau_x & \tau_y & \tau_z\end{bmatrix}^T$, and $\mathbf{W}$ is full rank matrix, see [2]. The translational dynamics is modeled by Newtons equations of motion which yields

$$\begin{bmatrix}\ddot{x}_e \\ \ddot{y}_e \\ \ddot{z}_e\end{bmatrix} = \begin{bmatrix}0 \\ 0 \\ g\end{bmatrix} - \mathbf{L}_{EB}\begin{bmatrix}0 \\ 0 \\ \frac{T}{m}\end{bmatrix} \tag{7}$$

where L_{EB} is the transformation matrix from B to E [20].

The angular velocity vector of Quadrotor in frame B with respect to E is denoted by $\mathbf{\Omega}$ and express in B as

$$\mathbf{\Omega} = \begin{bmatrix}p & q & r\end{bmatrix}^T \tag{8}$$

Then the Quadrotor's rotational kinematics is given by the relation between the time rates of Euler's angles and the body components of $\mathbf{\Omega}$ as [20]

$$\begin{bmatrix}\dot{\phi} \\ \dot{\theta} \\ \dot{\psi}\end{bmatrix} = \begin{bmatrix}1 & s_\phi t_\theta & c_\phi t_\theta \\ 0 & c_\phi & -s_\phi \\ 0 & s_\phi/c_\theta & c_\phi/c_\theta\end{bmatrix}\begin{bmatrix}p \\ q \\ r\end{bmatrix} \tag{9}$$

where t_θ stands for $\tan\theta$. In compact form, (9) is written as

$$\dot{\boldsymbol{\vartheta}} = \mathbf{\Gamma}(\phi, \theta)\mathbf{\Omega} \tag{10}$$

The angular momentum vector of the Quadrotor about its CG is $\mathbf{H} = \mathbf{J\Omega}$, where $\mathbf{J} = diag\begin{bmatrix}J_x, & J_y, & J_z\end{bmatrix}$ is the constant 3×3 diagonal body inertia matrix. The time derivative of $\mathbf{H}$ relative to E is given by the basic kinematical equation [21] as

$$\frac{^E d\mathbf{H}}{dt} = \frac{^B d\mathbf{H}}{dt} + \mathbf{\Omega} \times \mathbf{H} = \mathbf{J}\dot{\mathbf{\Omega}} + \mathbf{\Omega}^\times \mathbf{J\Omega} \tag{11}$$

where $\mathbf{\Omega}^\times$ is the skew symmetric matrix [1]. The rotational dynamics is modeled by Euler's equations of motion as

$$\frac{^E d\mathbf{H}}{dt} = \boldsymbol{\tau} \tag{12}$$

where $\boldsymbol{\tau} = \begin{bmatrix}\tau_x & \tau_y & \tau_z\end{bmatrix}^T$. Substituting (11) in (12) and solving for $\dot{\mathbf{\Omega}}$ yields the following rotational dynamical equations of motion in B

$$\dot{\mathbf{\Omega}} = -\mathbf{J}^{-1}\mathbf{\Omega}^\times \mathbf{J\Omega} + \mathbf{J}^{-1}\boldsymbol{\tau} \tag{13}$$

To have control input in (10), its derivative has been taken which yields

$$\ddot{\boldsymbol{\vartheta}} = \dot{\mathbf{\Gamma}}(\phi, \theta, \dot{\phi}, \dot{\theta})\mathbf{\Omega} + \mathbf{\Gamma}(\phi, \theta)\dot{\mathbf{\Omega}} \tag{14}$$

where $\dot{\mathbf{\Gamma}}(\phi, \theta, \dot{\phi}, \dot{\theta})$ is the time derivative of $\mathbf{\Gamma}(\phi, \theta)$. By solving (10), (13) and (14), we get

$$\ddot{\boldsymbol{\vartheta}} = \mathbf{F} + \mathbf{G}\boldsymbol{\tau} \tag{15}$$

where

$$\mathbf{F} = \dot{\mathbf{\Gamma}}\mathbf{\Gamma^{-1}}\dot{\boldsymbol{\vartheta}} + \mathbf{\Gamma}\{-\mathbf{J}^{-1}(\mathbf{\Gamma}^{-1}\dot{\boldsymbol{\vartheta}})^X \mathbf{J}\mathbf{\Gamma}^{-1}\dot{\boldsymbol{\vartheta}}\}, \tag{16}$$

$$\mathbf{G} = \mathbf{\Gamma J^{-1}} \tag{17}$$

III. Controller Architecture

The two-loop structured control system is proposed having slow (outer) loop and fast (inner) loop as shown in Fig. 2. The outer loop contains the positional state vector $\mathbf{x}_o = \begin{bmatrix}x_e & y_e & z_e\end{bmatrix}^T$, while the inner loop contains attitude state vector $\mathbf{x}_a = \begin{bmatrix}\phi & \theta & \psi\end{bmatrix}^T$ and body rate state vector $\mathbf{x}_r = \begin{bmatrix}p & q & r\end{bmatrix}^T$. In outer loop, PD control is designed, which generates the desired pitch and roll attitude commands based on longitudinal and lateral positional errors along with generating the required thrust to achieve the desired altitude. In the inner loop, AGDI control is implemented to follow the desired roll, pitch (generated by outer loop) and yaw attitude profiles, while stabilizing the angular body rates.

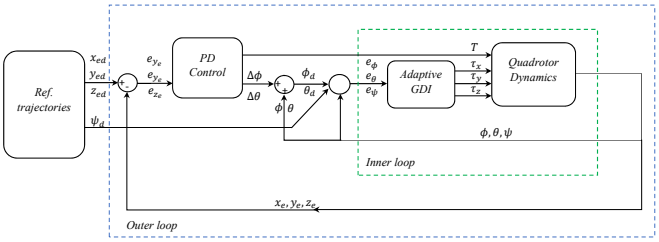

Fig. 2: Control architecture

IV. PD CONTROL FOR OUTER POSITION LOOP

To acquire the desired positions in x_e and y_e axis, the PD control is designed as

$$(\ddot{x}_e - \ddot{x}_{ed}) + c_1(\dot{x}_e - \dot{x}_{ed}) + c_2(x_e - x_{ed}) = 0 \tag{18}$$

$$(\ddot{y}_e - \ddot{y}_{ed}) + c_3(\dot{y}_e - \dot{y}_{ed}) + c_4(y_e - y_{ed}) = 0 \tag{19}$$

To generate θ_d and ϕ_d, the desired nonlinear dynamics of position x_e and y_e is linearized about the instantaneous values of θ and ϕ which yields

$$\begin{bmatrix} \ddot{x}_{ed} \\ \ddot{y}_{ed} \end{bmatrix} = - \begin{bmatrix} s_\psi s_{(\phi+\Delta\phi)} + c_\psi s_{(\theta+\Delta\theta)} c_{(\phi+\Delta\phi)} \\ -c_\psi s_{(\phi+\Delta\phi)} + s_\psi s_{(\theta+\Delta\theta)} c_{(\phi+\Delta\phi)} \end{bmatrix} \frac{T}{m} \tag{20}$$

where $\Delta\theta$ and $\Delta\phi$ are the attitude corrections in order to attain the desired position coordinates. By expanding the trigonometric functions of θ and ϕ about the instantaneous values of $\theta(t)$ and $\phi(t)$, yields the following linear approximate expressions

$$\begin{bmatrix} \ddot{x}_{ed} \\ \ddot{y}_{ed} \end{bmatrix} = \mathbf{M} \begin{bmatrix} \Delta\theta \\ \Delta\phi \end{bmatrix} + \mathbf{N} \tag{21}$$

where

$$\mathbf{M} = \frac{T}{m} \begin{bmatrix} c_\psi c_\phi + s_\psi s_\theta s_\phi & -s_\psi c_\theta c_\phi \\ -s_\psi c_\phi + c_\psi s_\theta s_\phi & -c_\psi c_\theta c_\phi \end{bmatrix}, \tag{22}$$

$$\mathbf{N} = \frac{T}{m} \begin{bmatrix} c_\psi s_\phi - s_\psi s_\theta s_\phi \\ -s_\psi s_\phi - c_\psi s_\theta c_\phi \end{bmatrix} \tag{23}$$

To extract $\Delta\theta$ and $\Delta\phi$, substitute (21) in (18) and (19), resulting in

$$\Delta\theta = \frac{m}{T} \left\{ \frac{(\ddot{x}_e - \mathbf{N}) + c_1(\dot{x}_e - \dot{x}_{ed}) \\ +c_2(x_e - x_{ed}) + s_\psi c_\phi c_\psi \Delta\phi}{c_\psi c_\phi + s_\psi s_\theta s_\phi} \right\} \tag{24}$$

$$\Delta\phi = \frac{m}{T} \left\{ \frac{(\ddot{y}_e - \mathbf{N}) + c_3(\dot{y}_e - \dot{y}_{ed}) + c_4(y_e - y_{ed}) \\ -(s_\psi c_\phi + c_\psi s_\theta s_\phi)\Delta\theta}{c_\psi c_\phi + s_\psi s_\theta s_\phi} \right\} \tag{25}$$

Finally the expressions for θ_d and ϕ_d are calculated by $\theta_d = \theta(t) + \Delta\theta$ and $\phi_d = \phi(t) + \Delta\phi$. Similarly to attain desired altitude, the PD control is defined as,

$$(\ddot{z}_e - \ddot{z}_{ed}) + c_5(\dot{z}_e - \dot{z}_{ed}) + c_6(z_e - z_{ed}) = 0 \tag{26}$$

where

$$\ddot{z}_e = -g + \frac{T\cos\theta\cos\phi}{m} \tag{27}$$

The required thrust T is evaluated by solving (26) and (27), resulting in

$$T = -\frac{m}{\cos\theta\cos\phi}[\ddot{z}_{ed} + g - c_5(\dot{z}_e - \dot{z}_{ed}) - c_6(z_e - z_{ed})] \tag{28}$$

V. GDI CONTROL FOR INNER ATTITUDE LOOP

To construct GDI, the expressions given by (13) and (15) are rewritten as

$$\dot{\mathbf{x}}_r = \mathbf{A}_r(\mathbf{x}_r, t) + \mathbf{B}_r\boldsymbol{\tau} \tag{29}$$

$$\ddot{\mathbf{x}}_a = \mathbf{F} + \mathbf{G}\boldsymbol{\tau} \tag{30}$$

where $\mathbf{A}_r = -\mathbf{J}^{-1}\boldsymbol{\Omega}^{\times}\mathbf{J}\boldsymbol{\Omega}$ and $\mathbf{B}_r = \mathbf{J}^{-1}$. The weighted error norm of the attitude state deviation function is defined as

$$\begin{aligned} \chi &= \|\mathbf{e}_a\|_w^2 = \kappa_1(\phi - \phi_d)^2 + \kappa_2(\theta - \theta_d)^2 + \kappa_3(\psi - \psi_d)^2 \\ &= \kappa_1 e_\phi^2 + \kappa_2 e_\theta^2 + \kappa_1 e_\psi^2 \end{aligned} \tag{31}$$

where $k_{1,2,3}$, are positive constants. The linear time varying constraint differential equation is formulated, the differential order of which is the same as the relative degree of the deviation function. The equation takes the following form

$$\ddot{\chi} + a_1(t)\dot{\chi} + a_2(t)\chi = 0 \tag{32}$$

where a_1 and a_2 are chosen such that the constraint dynamics is uniformly asymptotically stable. The time derivatives for constraint dynamics are computed as

$$\dot{\chi} = 2\mathbf{e}_a^T\mathbf{D}\dot{\mathbf{e}}_a \tag{33}$$

$$\ddot{\chi} = 2\mathbf{e}_a^T\mathbf{D}[\mathbf{F} + \mathbf{G}\boldsymbol{\tau} - \ddot{\mathbf{x}}_{ed}] + 2\dot{\mathbf{e}}_a^T\mathbf{D}\dot{\mathbf{e}}_a \tag{34}$$

where $\mathbf{D}$ represents the 3×3 diagnonal matrix with $\kappa_1, \kappa_2, \kappa_3$ are its diagonal elements. By placing the time derivatives in (32), the algebraic form is written as

$$\mathcal{A}(\mathbf{x}_a, \mathbf{x}_r, t)\boldsymbol{\tau} = B(\mathbf{x}_a, \mathbf{x}_r, t) \tag{35}$$

where,

$$\mathcal{A}(\mathbf{x}_a, \mathbf{x}_r, t) = 2\mathbf{e}_a^T\mathbf{D}\mathbf{G}, \tag{36}$$

$$\begin{aligned} B(\mathbf{x}_a, \mathbf{x}_r, t) &= -2\dot{\mathbf{e}}_a^T\mathbf{D}\dot{\mathbf{e}}_a - 2a_1\mathbf{e}_a^T\mathbf{D}\dot{\mathbf{e}}_a - a_2\mathbf{e}_a^T\mathbf{D}\mathbf{e}_a \\ &\quad -2\mathbf{e}_a^T\mathbf{D}F + 2\mathbf{e}_a^T\mathbf{D}\ddot{\mathbf{x}}_{ed} \end{aligned} \tag{37}$$

Equation (35) is an under-determined algebraic system having infinite number of solutions. These solutions are parameterized by generalized inversion using the Greville formula, which yields

$$\boldsymbol{\tau} = \mathcal{A}^+(\mathbf{x}_a, \mathbf{x}_r, t)B(\mathbf{x}_a, \mathbf{x}_r, t) + \mathbf{P}(\mathbf{x}_a, \mathbf{x}_r, t)\boldsymbol{\zeta} \tag{38}$$

where $\mathcal{A}^+$ is the MPGI, $\boldsymbol{\zeta} \in R^3$ is null control vector, and $\mathbf{P}$ is the null projection matrix given by

$$\mathbf{P}(\mathbf{x}_a, \mathbf{x}_r, t) = \mathbf{I}_{3\times3} - \mathcal{A}^+(\mathbf{x}_a, \mathbf{x}_r, t)\mathcal{A}(\mathbf{x}_a, \mathbf{x}_r, t) \tag{39}$$

However, during generalized inversion, singularity problem arises when the inverted matrix tends to change its rank,

which causes discontinuity in the MPGI matrix function, and causes the elements of the MPGI matrix to go unbounded. In this paper, the Extended Generalized Dynamic Inverse method [19], is utilized to tackle the problem of GDI singularity.

A. Singularity avoidance

To avoid singularity, a first order dynamic scaling factor is augmented in MPGI [11], resulting in

$$\dot{\nu}(t) = -\nu(t) + \frac{\gamma \left\|\mathbf{e}_r(t)\right\|^2}{\left\|\mathbf{e}_a(t)\right\|^2},\ \nu(0) > 0 \tag{40}$$

where γ is a positive real valued constant and $\mathbf{e}_r = \left[p - p_d(t)\ q - q_d(t)\ r - r_d(t)\right]^T$. Now the modified generalized inverse $\mathcal{A}^*(\mathbf{x}_a, \mathbf{x}_r, \nu, t)$ is written as

$$\begin{aligned}\mathcal{A}^*(\mathbf{x}_a, \mathbf{x}_r, \nu, t) &= \mathcal{A}^T(\mathbf{x}_a, \mathbf{x}_r, t)\big\{\mathcal{A}(\mathbf{x}_a, \mathbf{x}_r, t) \\ &\quad \mathcal{A}^T(\mathbf{x}_a, \mathbf{x}_r, t) + \nu(t)\big\}^{-1}\end{aligned} \tag{41}$$

The amended form of GDI control expression is given as

$$\boldsymbol{\tau}^* = \mathcal{A}^*(\mathbf{x}_a, \mathbf{x}_r, \nu, t)B(\mathbf{x}_a, \mathbf{x}_r, t) + \mathbf{P}(\mathbf{x}_a, \mathbf{x}_r, t)\boldsymbol{\zeta} \tag{42}$$

The detailed proof of the elements of $\mathcal{A}^*$ are bounded for all $t > 0$ is found in [11].

B. Null control vector design

The null control vector $\boldsymbol{\zeta}$ is designed to assure global closed-loop stability of the body rate dynamics, which is defined as

$$\mathbf{P}\boldsymbol{\zeta} = -\big(\bar{\mathbf{P}}\mathbf{B}_r\big)^{-1}\mathbf{P}\left(\bar{\mathbf{P}}\boldsymbol{\Delta}_i + 0.5\dot{\mathbf{P}}\mathbf{e}_r + 0.5\mathbf{Q}\mathbf{e}_r\right) \tag{43}$$

By placing the value of $\boldsymbol{\zeta}$ in (42), the control law takes the following form

$$\boldsymbol{\tau}^* = \mathcal{A}^*B - (\bar{\mathbf{P}}\mathbf{B}_r)^{-1}\mathbf{P}\left(\bar{\mathbf{P}}\boldsymbol{\Delta}_i + 0.5\dot{\mathbf{P}}\mathbf{e}_r + 0.5\mathbf{Q}\mathbf{e}_r\right) \tag{44}$$

Theorem 5.1: The control law given by (44) guarantees global closed-loop stability of the body rate dynamics.

Proof: Let the null control vector $\boldsymbol{\zeta}$ is designed to be a linear function of body rate error vector, defined as

$$\boldsymbol{\zeta} = \mathbf{K}\mathbf{e}_r = \mathbf{K}(\mathbf{x}_r - \mathbf{x}_{rd}) \tag{45}$$

The error dynamics of inner state vector is obtained by subtracting $\dot{\mathbf{x}}_r$ from $\dot{\mathbf{x}}_{rd}(t)$, which yields

$$\begin{aligned}\dot{e}_r &= \mathbf{A}_r\left(\mathbf{x}_r, t\right) - \mathbf{A}_r\left(\mathbf{x}_{rd}, t\right) + \mathbf{B}_r\{\mathcal{A}^*(\mathbf{x}_a, \mathbf{x}_r, \nu, t) \\ &\quad B(\mathbf{x}_a, \mathbf{x}_r, t) + \mathbf{P}(\mathbf{x}_a, \mathbf{x}_r, t)\mathbf{K}\mathbf{e}_r\} \\ &\quad -\mathbf{B}_r\{\mathcal{A}^*(\mathbf{x}_a, \mathbf{x}_{rd}, t)B(\mathbf{x}_a, \mathbf{x}_{rd}, t)\}\end{aligned} \tag{46}$$

The error dynamics given by (46) is written compactly as

$$\dot{\mathbf{e}}_r = \boldsymbol{\Delta}_r\left(\mathbf{x}_a, \mathbf{x}_r, \mathbf{x}_{rd}\right) + \mathbf{B}_r\mathbf{P}(\mathbf{x}_a, \mathbf{x}_r, t)\mathbf{K}\mathbf{e}_r \tag{47}$$

Now consider the control Lyapunov function

$$V\left(\mathbf{x}_a, \mathbf{x}_r, t\right) = {\mathbf{e}_r}^T\bar{\mathbf{P}}(\mathbf{x}_a, \mathbf{x}_r, t)\mathbf{e}_r \tag{48}$$

where the matrix $\bar{\mathbf{P}}(\mathbf{x}_a, \mathbf{x}_r, t) = \mathbf{P} + \epsilon\mathbf{I}_{3\times 3}$ is symmetric positive definite, in which ϵ is an arbitrary positive real scalar. The derivative of the Lyapunov function is given as

$$\dot{V} = {\mathbf{e}_r}^T(2\bar{\mathbf{P}}\boldsymbol{\Delta}_r + 2\bar{\mathbf{P}}B_r\mathbf{P}\mathbf{K}\mathbf{e}_r + \dot{\mathbf{P}}\mathbf{e}_r) \tag{49}$$

For asymptotic stability, the condition $\dot{V}{<}0\ \forall\ \mathbf{e}_r \neq 0$ must be satisfied. This can be assured by the existence of symmetric positive definite matrix $\mathbf{Q}$ such that

$$\dot{V} = -{\mathbf{e}_r}^T\mathbf{Q}\mathbf{e}_r < 0 \tag{50}$$

Equating (49) with (50) yields

$$\left(2\bar{\mathbf{P}}\boldsymbol{\Delta}_r + 2\bar{\mathbf{P}}\mathbf{B}_r\mathbf{P}\mathbf{K}\mathbf{e}_r + \dot{\mathbf{P}}\mathbf{e}_r + \mathbf{Q}\mathbf{e}_r\right) = 0 \tag{51}$$

The value of the projected gain $\mathbf{P}\mathbf{K}\mathbf{e}_r$ is solved for from (51) as

$$\mathbf{P}\boldsymbol{\zeta} = -\big(\bar{\mathbf{P}}\mathbf{B}_r\big)^{-1}\mathbf{P}\left(\bar{\mathbf{P}}\boldsymbol{\Delta}_r + 0.5\dot{\mathbf{P}}\mathbf{e}_r + 0.5\mathbf{Q}\mathbf{e}_r\right) \tag{52}$$

The null control vector given by (52) guarantees the asymptotic stability of body rate dynamics. ■

VI. Design of AGDI control system

In this paper, an adaptive form of GDI control law is formulated by the augmentation of SMC based robust term, resulting in

$$\boldsymbol{\tau}^* = \mathcal{A}^*B + \mathbf{P}\boldsymbol{\zeta} - C\mathcal{A}^*\frac{s}{\|s\|} \tag{53}$$

where C denotes the adaptive modulation gain to enforce sliding, defined as

$$C = \|\mathbf{u}_{eq}\|\hat{C} + \eta \tag{54}$$

where $\|\mathbf{u}_{eq}\| = \mathcal{A}^*B + \mathbf{P}\boldsymbol{\zeta}$ and η is a constant, which ensures the reaching condition. The positive adaptation gain $\hat{C}$ evolves according to

$$\dot{\hat{C}} = -g_1\hat{C} + g_2\varepsilon_0\|\mathbf{u}_{eq}\|\|s\| \tag{55}$$

where g_1, g_2 and ε_0 are constant positive scalar gains and s is the sliding surface defined as

$$s = \dot{\chi} + a_1(t)\chi + a_2(t)\int \chi dt \tag{56}$$

The time derivative of the sliding surface s is given as

$$\dot{s} = \ddot{\chi} + a_1(t)\dot{\chi} + a_2(t)\chi \tag{57}$$

By solving (57) we have

$$\dot{s} = \mathcal{A}(\mathbf{x}_a, \mathbf{x}_r, t)\boldsymbol{\tau}^* - B(\mathbf{x}_a, \mathbf{x}_r, t) \tag{58}$$

A. Stability analysis of AGDI control

To prove the stability of AGDI control law, the value of $\boldsymbol{\tau}^*$ expressed by (53) is placed in (58), which yields

$$\dot{s} = \mathcal{A}\big\{\mathcal{A}^*B + \mathbf{P}\boldsymbol{\zeta} - C\mathcal{A}^*\frac{s}{\|s\|}\big\} - B \tag{59}$$

Furthermore, place the expression of null projection matrix $\mathbf{P}$ given by (39), and evoking the property of pseudo inverse, i.e. $\mathcal{A}\mathcal{A}^+ = \mathbf{1}$, for all $\mathcal{A}(\mathbf{x}_a, \mathbf{x}_r, t) \neq \mathbf{0}_{1\times 3}$, the expression of $\dot{s}$ given by (59) curtails to

$$\dot{s} = \{\rho_A(\mathbf{x}_a, \mathbf{x}_r, \nu, t) - 1\}B - C\rho_{\mathcal{A}}(\mathbf{x}_a, \mathbf{x}_r, \nu, t)\frac{s}{\|s\|} \tag{60}$$

where $\rho_{\mathcal{A}} = \mathcal{A}(\mathbf{x}_a, \mathbf{x}_r, t)\mathcal{A}^*(\mathbf{x}_a, \mathbf{x}_r, \nu, t)$. However the identity $\mathcal{A}\mathcal{A}^+ = \mathbf{1}$ does not hold true for $\rho_{\mathcal{A}}$. Nevertheless, because $\nu \in (0, \infty)$, it follows from the definition of $\mathcal{A}^*(\mathbf{x}_a, \mathbf{x}_r, \nu, t)$ given by (41) that

$$0 < \rho_{\mathcal{A}}(\mathbf{x}_a, \mathbf{x}_r, \nu, t) < 1 \tag{61}$$

for all $\mathcal{A}(\mathbf{x}_a, \mathbf{x}_r, t) \neq \mathbf{0}_{1\times 3}$ and that

$$\lim_{t\to\infty} \rho_{\mathcal{A}}(\mathbf{x}_a, \mathbf{x}_r, \nu, t) = 0 \Leftrightarrow \lim_{t\to\infty} \mathcal{A}(\mathbf{x}_a, \mathbf{x}_r, t) = \mathbf{0}_{1\times 3} \tag{62}$$

The following positive definite candidate Lyapunov function

$$V = \frac{1}{2}s^2$$

will be employed to design the adaptive sliding gain C. The time derivative of the Lyapunov function is evaluated as

$$\dot{V} = s\dot{s} = s\{\rho_{\mathcal{A}} - 1\}B - Cs\rho_{\mathcal{A}}\frac{s}{\|s\|} \tag{63}$$

Therefore, a function $C(\mathbf{x}_a, \mathbf{x}_r, \nu, t)$ that ensures

$$C(\mathbf{x}_a, \mathbf{x}_r, \nu, t) = \|\mathbf{u}_{eq}\|\hat{C} + \eta > \frac{\rho_{\mathcal{A}} - 1}{\rho_{\mathcal{A}}}B\frac{s}{\|s\|} \tag{64}$$

would guarantee the negative definiteness of $\dot{V}$, which will assure the finite time stability of $s = 0$ follows from Lyapunov's direct method [22]. This will also ensures finite time stability of $\mathbf{e}_a = \mathbf{0}_{3\times 1}$ as obvious from the definition of s given by (56). Hence, it follows from the definition of $\mathcal{A}(\mathbf{x}_a, \mathbf{x}_r, t)$ given by (36) along with the condition given by (62) that $\rho_{\mathcal{A}}(\mathbf{x}_a, \mathbf{x}_r, \nu, t)$ must also converge to zero. Therefore,

$$\lim_{\mathbf{e}_r\to\mathbf{0}_{3\times 1}} \frac{\rho_{\mathcal{A}}(\mathbf{x}_a, \mathbf{x}_r, \nu, t) - 1}{\rho_{\mathcal{A}}(\mathbf{x}_a, \mathbf{x}_r, \nu, t)} = -\infty \tag{65}$$

which requires the function $C(\mathbf{x}_a, \mathbf{x}_r, \nu, t)$ or η to reach infinite values as $\mathbf{e}_r$ vanishes in order to guarantee $\dot{V} < 0$ and $s = 0$. Therefore it is not possible to guarantee the finite time closed-loop stability of sliding mode dynamics given by (60), however it is feasible to achieve the semi-global practical stability of the GDI sliding mode dynamics via SMC gain design.

Theorem 6.1: There exists a real number $\eta^* > 0$ for every real number $\rho^*_{\mathcal{A}} \in (0, 1)$ which ensures the negative definiteness of $\dot{V}$ along the solution trajectories of the sliding mode dynamics given by (60) for all $\rho_{\mathcal{A}}(\mathbf{x}_a, \mathbf{x}_r, \nu, t) > \rho^*_{\mathcal{A}}$ and $\eta > \eta^*$.

Proof: Let $\rho^*_{\mathcal{A}}$ be a prescribed constant real scalar in the range of $\rho_{\mathcal{A}}(\mathbf{x}_a, \mathbf{x}_r, \nu, t)$, i.e., $\rho^*_{\mathcal{A}} \in (0, 1)$. Also, define $\bar{\eta}(\mathbf{x}_a, \mathbf{x}_r, t)$ as

$$\bar{\eta}(\mathbf{x}_a, \mathbf{x}_r, t) = -\frac{\rho^*_{\mathcal{A}} - 1}{\rho^*_{\mathcal{A}}}|B(\mathbf{x}_a, \mathbf{x}_r, t)| \tag{66}$$

It follows that $\bar{\eta}(\mathbf{x}_a, \mathbf{x}_r, t) > \eta(\mathbf{x}_a, \mathbf{x}_r, \nu, t)$ whenever $\rho_{\mathcal{A}}(\mathbf{x}_a, \mathbf{x}_r, \nu, t) > \rho^*_{\mathcal{A}}$. Accordingly, let $\mathcal{D}$ be a neighborhood of $(\mathbf{e}_a, \mathbf{e}_r) = (\mathbf{0}_3, \mathbf{0}_3)$, and choose a sliding gain constant η^* such that

$$\eta^* > \max_{\mathcal{D}} \bar{\eta}(\mathbf{x}_a, \mathbf{x}_r, t) \tag{67}$$

TABLE I: X-4 Flyer Quadrotor specifications

Parameters	Description	Value
m	mass	4
d	arm length	0.315
J_x, J_y	inertia	0.0820
J_z	inertia	0.1490
b	thrust factor	$1.323e^{-5}$
k	drag factor	$1.069e^{-7}$

Then the negative definiteness of $\dot{V} < 0$ holds true along any closed loop trajectory that originates within $\mathcal{D}$ whenever $\rho_{\mathcal{A}}(\mathbf{x}_a, \mathbf{x}_r, \nu, t) \geq \rho^*_{\mathcal{A}}$ and $\eta > \eta^*$. The existence of a finite number η^* is guaranteed for any domain $\mathcal{D}$ because $B(\mathbf{x}_a, \mathbf{x}_r, t)$ is globally bounded by virtue of implementing the DSGI $\mathcal{A}^*$ given by (41), which result in globally bounded $\mathbf{e}_a$ trajectories. ■

Remark 1: It follows from Theorem 6.1 that the magnitude of the positive sliding mode gain constant η can always be increased such that an arbitrarily small positive bound $\rho^*_{\mathcal{A}}$ is achieved with guaranteeing the condition $\dot{V} < 0$ to hold over $\mathcal{D}$ whenever $\rho_{\mathcal{A}}(\mathbf{x}_a, \mathbf{x}_r, \nu, t) < \rho^*_{\mathcal{A}}$. Since the attitude error state trajectory $\mathbf{e}_a$ must enter the domain defined by $\rho_{\mathcal{A}}(\mathbf{x}_a, \mathbf{x}_r, \nu, t) < \rho^*_{\mathcal{A}}$ in finite time and remain within that domain, it follows that driving $\rho^*_{\mathcal{A}}$ arbitrarily closer to zero implies driving $\mathbf{e}_a$ arbitrarily closer to zero and making it uniformly ultimately bounded, i.e., making $\mathbf{e}_a = \mathbf{0}_{3\times 1}$ practically stable. Moreover, because $\mathcal{D}$ can be arbitrarily enlarged by increasing η^*, then this practical stability is semi-global.

VII. Simulation results

To analyze the performance of proposed control methodology, the parameters of X-4 flyer Quadrotor are used to model the vehicle, whose specifications are given in Table I, see [1]. Numerical simulations are conducted for the following scenarios.

A. Waypoints following

In this plot, the aerial vehicle is commanded to follow the pre-defined waypoints. Simulation result shown by Fig. 3a and 3b, reveals that the vehicle has successfully achieved the desired positional coordinates. The attitude profiles are shown in Fig. 3c, whereas the control commands are illustrated in Fig. 3d.

B. Helical trajectory tracking

In this scenario, the reference helical trajectory is commanded such that $x_{ed} = 10\sin 2\pi ft$, $y_{ed} = 10\cos 2\pi ft$ with increasing altitude upto $z_{ed} = 200m$, to examine the tracking capability in the presence of continuous wind field shown by Fig. 4a, and by applying -10% variation in the parameters such as mass, moment of inertia, aerodynamic thrust and drag coefficients and arm length. The trajectory tracking performance is shown in Fig. 4b, whereas the actual and desired attitudes profiles are shown in Fig. 4c. The corresponding control deflections are shown in Fig. 4d, which demonstrate that the proposed control law is quiet effective and robust.

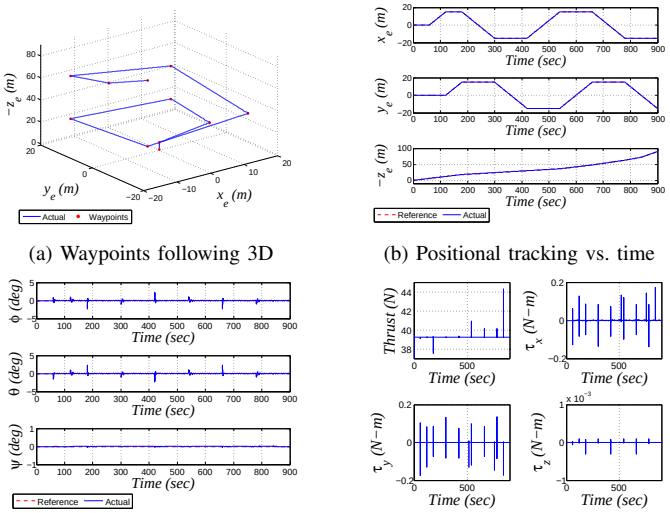

(a) Waypoints following 3D (b) Positional tracking vs. time

(c) Attitude angles vs. time (d) Control commands vs. time

Fig. 3: Waypoints following

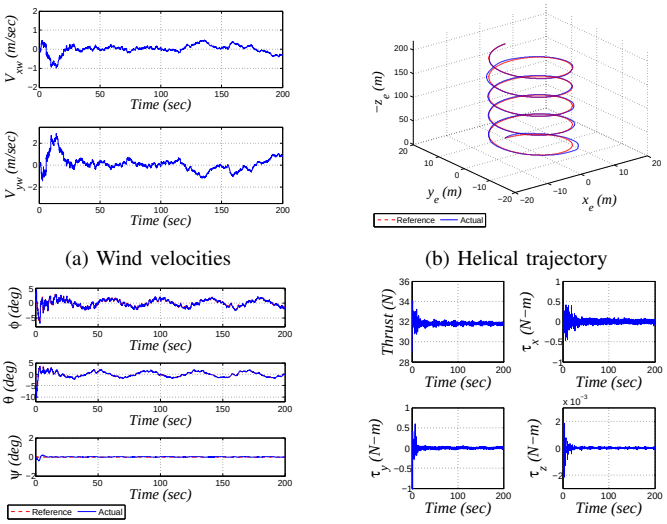

(a) Wind velocities (b) Helical trajectory

(c) Attitude angles vs. time (d) Control commands vs. time

Fig. 4: Helical trajectory tracking

VIII. Conclusion

In this paper, the two-loop structured control system is designed for position and attitude control of multi-rotor aerial vehicle. The PD control, successfully generates the required pitch and roll attitude commands based on positional errors while tracking the desired altitude. In the inner loop, AGDI control having SMC term, successfully tracks the desired attitude profiles such that the tracking errors are proven to ultimately converge to the given neighborhoods of the origin, guaranteeing semi-global practically stable attitude tracking. The singularity problem is solved by implementing the dynamic scale factor. The null control vector is designed to stabilize the inner body rate dynamics. Numerical simulations successfully demonstrate the efficiency and robustness attributes of proposed control approach.

References

[1] P. Corke, *Robotics, vision and control: fundamental algorithms in MATLAB*. Springer, 2011, vol. 73.

[2] R. Mahony, V. Kumar, and P. Corke, "Multirotor aerial vehicles: Modeling, estimation, and control of quadrotor. roboticsautomationmagazine, 19, 20-32," *Mayhew et al. C. Mayhew, R. Sanfelice, and A. Teel. On path-lifting mechanisms and unwinding in quaternion-based attitude control. Automatic Control, IEEE Transactions on. PP (99)*, pp. 1–1, 2012.

[3] S. Bouabdallah, A. Noth, and R. Siegwart, "Pid vs lq control techniques applied to an indoor micro quadrotor," in *Intelligent Robots and Systems, 2004.(IROS 2004). Proceedings. 2004 IEEE/RSJ International Conference on*, vol. 3. IEEE, 2004, pp. 2451–2456.

[4] S. Bouabdallah and R. Siegwart, "Full control of a quadrotor," in *Intelligent robots and systems, 2007. IROS 2007. IEEE/RSJ international conference on*. IEEE, 2007, pp. 153–158.

[5] A. Benallegue, A. Mokhtari, and L. Fridman, "Feedback linearization and high order sliding mode observer for a quadrotor uav," in *Variable Structure Systems, 2006. VSS'06. International Workshop on*. IEEE, 2006, pp. 365–372.

[6] N. I. Vitzilaios and N. C. Tsourveloudis, "An experimental test bed for small unmanned helicopters," *Journal of Intelligent and Robotic Systems*, vol. 54, no. 5, pp. 769–794, 2009.

[7] K. Alexis, G. Nikolakopoulos, and A. Tzes, "Experimental model predictive attitude tracking control of a quadrotor helicopter subject to wind-gusts," in *Control & Automation (MED), 2010 18th Mediterranean Conference on*. IEEE, 2010, pp. 1461–1466.

[8] M. L. Ireland, A. Vargas, and D. Anderson, "A comparison of closed-loop performance of multirotor configurations using non-linear dynamic inversion control," *Aerospace*, vol. 2, no. 2, pp. 325–352, 2015.

[9] J. O. Pedro, A. Panday, and L. Dala, "A nonlinear dynamic inversion-based neurocontroller for unmanned combat aerial vehicles during aerial refuelling," *International Journal of Applied Mathematics and Computer Science*, vol. 23, no. 1, pp. 75–90, 2013.

[10] U. Ansari and A. Bajodah, "Robust launch vehicles generalized dynamic inversion attitude control," *Aircraft Engineering and Aerospace Technology*, no. just-accepted, pp. 00–00, 2017.

[11] U. Ansari and A. H. Bajodah, "Robust generalized dynamic inversion based control of autonomous underwater vehicles," *Proceedings of the Institution of Mechanical Engineers, Part M: Journal of Engineering for the Maritime Environment*, p. 1475090217708640, 2017.

[12] ——, "Robust generalized dynamic inversion quadrotor control," *IFAC-PapersOnLine*, vol. 50, no. 1, pp. 8181–8188, 2017.

[13] ——, "Robust generalized inversion control: An application to satellite launch vehicle attitude control," *International Journal of Control Theory and Applications*, vol. 10, no. 34, pp. 93–110, 2017.

[14] ——, "Robust generalized dynamic inversion control of autonomous underwater vehicles," *IFAC-PapersOnLine*, vol. 50, no. 1, pp. 10 658–10 665, 2017.

[15] U. Ansari, A. H. Bajodah, and S. Alam, "Generalized dynamic inversion based attitude control of autonomous underwater vehicles," *IFAC-PapersOnLine*, vol. 49, no. 23, pp. 582–589, 2016.

[16] U. Ansari and A. H. Bajodah, "Guidance and robust generalized inversion based attitude control of satellite launch vehicle," in *Control Engineering & Information Technology (CEIT), 2016 4th International Conference on*. IEEE, 2016, pp. 1–6.

[17] ——, "Quadrotor control using generalized dynamic inversion and terminal sliding mode," in *Control, Engineering & Information Technology (CEIT), 2015 3rd International Conference on*. IEEE, 2015, pp. 1–6.

[18] ——, "Generalized dynamic inversion scheme for satellite launch vehicle attitude control," *IFAC-PapersOnLine*, vol. 48, no. 9, pp. 114–119, 2015.

[19] I. Hameduddin and A. H. Bajodah, "Nonlinear generalised dynamic inversion for aircraft manoeuvring control," *International Journal of Control*, vol. 85, no. 4, pp. 437–450, 2012.

[20] R. Nelson, *Flight Stability and Automatic Control*, 2nd ed. McGraw-Hill, New York, 1997.

[21] N. J. Kasdin and D. A. Paley, *Engineering Dynamics*. Princeton University Press, 2011.

[22] H. K. Khalil, *Noninear Systems*. Prentice-Hall, New Jersey, 1996.